



I N T E G R A T E D
ENGINEERING SOFTWARE

**Towards Function Magnetic Stimulation (FMS)
Theory and Experiment**

Submitted to

IEEE Transactions on Biomedical Engineering

By

Kent Davey and Lanbo Luo
School of Electrical Engineering
Georgia Institute of Technology
Atlanta, GA 30332-0250

and

David Ross
VA Medical Center
Rehab R&D – 153
1670 Clairmont Road
Decatur, GA 30332-0250

February 13, 1993

Abstract

This paper examines the use of magnetic fields to functionally stimulate peripheral nerves. All electric fields are induced via a changing magnetic field whose flux is entirely confined within a closed magnetic circuit. Induced electric fields are stimulated using a nonlinear boundary element solver. The induced fields are solved using duality theory. The accuracy of these predictions is verified by saline bath experiments. Next the theory is applied to the stimulation of nerves using small, partially occluded ferrite and laminated vanadium permendur cores. Experiments demonstrate the successful stimulation of peripheral nerves in the African bullfrog with 11 mA, 153 mV excitations. These results offer a new vista of possibilities in the area of functional nerve stimulation. Unlike functional electric stimulation (FES), FMS does not involve any half cell reactions, and thus would not have the commensurate restrictions regarding balanced biphasic stimulation, strength duration balances, and oxidation issues, always exercising care that the electrodes remain in the reversible operating regime.

Introduction

Magnetic stimulation of nerves has classically been approached using external stimulators noninvasively exciting nerves in both the central and peripheral nervous system [1] [2]. The coils are typically air core ovals or D-shaped windings excited with exponentially decaying voltage obtained with a capacitive discharge. Most researchers compute the field from the coils using elliptic integrals; the internal field consistent with such a magnetic field in a semi-infinite isotropic conducting medium is simply the time rate of change of the magnetic vector potential so obtained [3]. When the medium is not semi-infinite, surface charge accumulates at interfaces having dissimilar conductivity. Davey [4] suggests two gauge transformations useful for easily accounting for these interfacial charges.

In the case of selective internal magnetic stimulation, the problem is altered in that the primary magnetic field is generally well known; it is the induced electric fields and the effect of interfaces that remains the problem. Although the use of closed magnetic torroid loops have been suggested as potentially useful for stimulating nerves [5], the authors were not successful in stimulating nerves magnetically.

Until this team employed high permeability, high saturation torroids with partially occluded central openings to focus the electric field, we were not successful in stimulating nerves. The torroids used are made of orthinol or vanadium permendur. Because the magnetic circuit is so good, a large flux is invoked in the core with every little current. This changing flux induces an E field which threads through the center of the torroid core.

Recent research with nerve excitation models clearly identifies the fact that long nerve fibers fire according to the coaxial electric field gradient, having a threshold near 13 mv/mm_2 , while short fibers respond to the local electric field [6], [7].

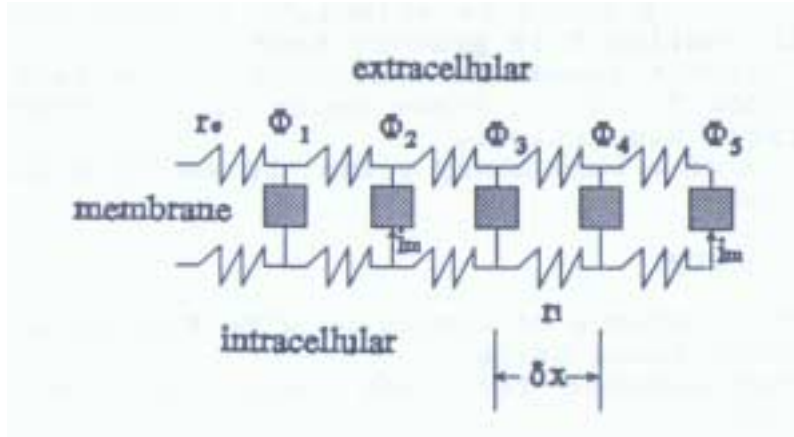


Figure 1: Schematic circuit of a nerve fiber. When the nerve fiber is below subthreshold, the boxes represent the parallel resistance and capacitance of the membrane. Above threshold they represent the Hodgkin Huxley action potential circuit.

This is easily demonstrated by the drawing in Figure 1 in terms of the external potentials Φ . The membrane current i_m at node 2 is

$$i_m = -\frac{\partial}{\partial x} \left(\frac{r_e (\Phi_3 + \Phi_1 - 2\Phi_2)}{\partial x} \right) = -\frac{\partial}{\partial x} \left(\frac{\partial E_x}{\partial x} \right) \quad (1)$$

At the end of the fiber circuit model, at node 5, the membrane current i_m is given as

$$i_m = -\frac{(\Phi_4 - \Phi_5)}{r_e \delta x} = \frac{1}{r_e} E_x \quad (2)$$

The determination of when a fiber is long is not clear, but a first approximation is suggested by examining the “cable” impedance of the fiber and comparing it to a fiber of infinite length as described by Plonsey and Barr [8]. Using cable impedance concepts the case is established that a fiber is considered long when $L \geq 3\lambda$, where λ is a length parameter equal to the ratio of membrane resistance to the sum of extracellular and intracellular resistance (on a per unit length

basis), i.e., $\lambda = \sqrt{\frac{r_m}{r_i + r_e}}$.

Within this backdrop of information, the problem remains to design and test a magnetic stimulator capable of realizing a coaxial electric field gradient of greater than 13 mv/mm^2 . From experience, the team found this requirement more demanding than attempting to realize an E field to stimulate a short fiber. The subtasks required to realize this primary task are

- Define magnetic circuit geometries suitable to the task.
- Simulate the induced field for these geometries numerically.
- Verify the numerical simulations.
- Test the stimulator on a laboratory animal to verify stimulation of an action potential.

Magnetic Circuit Geometry

If FMS is to have a chance of competing with FES, it must meet several criteria, among those being

- a. Small current requirements for long range implantation and heating considerations.
- b. Small size and weight to fit around a nerve or nerve bundle.
- c. Flexibility of secondary suppression capability.

New developments in FES validate the need to preferentially stimulate smaller nerve fibers to the exclusion of larger ones. This is usually accomplished by employing a tripolar cuff type electrode. Any MFS stimulator should have the same capability of preferentially hyperpolarizing a portion of nerve fiber.

After analyzing several alternatives this team determined that the torroid type core is capable of meeting these criteria. In its simplest form, that adopted in these experiments, the core is simply a doughnut shaped torroid laminated by winding as a spool on a mandrel. Typical dimensions for this work were OD=1.9cm, ID=1.27cm, and height H=0.63 cm.

Because it is necessary to have both a high permeability and high saturation limit, the core material choices were vanadium permendur and orthinol. Recall that the objective in firing a nerve is realized by transferring charge through the membrane. As will be discussed shortly in detail, the induced E field is proportional to the time rate of change of the B field. The torroids used were stimulated by a sinusoidal voltage. Although a core can be excited above saturation, once the core goes into saturation, the commensurate induced E field is nearly zero. The E field representing charge transfer across the membrane is smaller than below saturation. Based on these results, we determined to drive our core sinusoidally just up to saturation. The high permeable, high saturation cores allowed us to work with smaller physical structures while still carrying the flux needed to fire a nerve.

In the torroid geometry, the nerve ideally runs through the center. It would appear on first glance that the cores would not be easily suited for placement around an intact nerve. A folded torroid is however quite suited. Because the permeability is so high, little flux leakage accompanies such a folding.

Induced Field Predictions

In the design stage of these devices it is critical to have an accurate simulation tool for accurately predicting the induced electric field. The simulation must accurately account for the shape and proximity of nonconducting boundaries such as the torroid core itself (which was painted with a thin silicone type coating to avoid shorting the desired E field) and the confines of our test chamber upon which induced charges accumulate to insure that $\hat{n} \cdot \vec{J} = 0$ where \hat{n} represents the unit normal to the nonconducting surface. The problem fits into a special class of eddy current problems for two reasons. First, the induced currents do not themselves perturb the primary magnetic field, because they are too weak. Second, the magnetic circuit of the primary field is extremely well defined, as dictated by the first requirement of small current in the above section. Thus the primary B field is easily determined. Although this is the case in this experiment, the field predictive scheme is easily adapted when it is not.

This subclass of eddy current problem is most easily solved using a static magnetic field solver to determine the induced electric field and current. The solution is realized through duality. In the most general problem where the B field is not well defined, the B field must necessarily be determined first. The induced fields are computed in a two step process – calculating the magnetic field first and then the E field. Both steps are computed with the same magnetic field solver. Because the induced fields do not alter the primary B field, the calculation of E is found

from Faraday’s law in terms of a known B, i.e., $\nabla \times \vec{E} = -\frac{\partial \vec{B}}{\partial t}$, maintaining the solenoidal property

of current density $\nabla \cdot \vec{J} = 0$ and the boundary condition $\hat{n} \cdot \vec{J} = 0$. In a sinusoidal problem with angular frequency ω , it is convenient to make a comparison table between typical magnetostatic equations and those governing the computation of E and J.

Table I Dual Relationships in Magneto – and Electroquasistatics

Magnetostatic	Induced E Field	Dual Relationships
$\nabla \times \vec{H} = \vec{J}$	$\nabla \times \vec{E} = -j\omega \vec{B}$	$\vec{E} \Rightarrow \vec{H}$
$\oint \vec{H} \cdot d\vec{l} = NI$	$\oint \vec{E} \cdot d\vec{l} = j\omega \Phi$	$j\omega \Phi \Rightarrow NI$
$\vec{B} = \mu \vec{H}$	$\vec{J} = \sigma \vec{E}$	$\sigma \Rightarrow \mu$
$\nabla \cdot \vec{B} = 0$	$\nabla \cdot \vec{J} = 0$	$\vec{J} \Rightarrow -j\omega \vec{B}$

The symbol Φ refers to magnetic flux. Once the driving magnetic field is known, the induced E field and current computation step 2 can be computed using the transference relationships dictated in the third column of Table I.

A boundary element solver is used in both analyses. The magnetic vector potential is represented in terms of a fictitious surface current. This current is placed on every interface where a discontinuity in permeability exists (this translates to a discontinuity in conductivity in the second E field computation step). It should be clear that the product $\omega \Phi$, takes the place of current in the conventional solver.

As discussed in a recent paper, Roger Harrington [9] shows that a dielectric or magnetizable body can always be represented by a skin of equivalent electric and magnetic currents. In magnetostatics the magnetizable body can be completely represented by a set of surface currents. Once these equivalent currents are determined, the magnetic body can be removed and replaced by a “sack of air” covered by this surface shroud of current. The question remains as to how to predict the correct equivalent surface current sheath. In magnetostatics, we seek the solution of the vector potential due to source currents such that

$$\vec{B} = \nabla \times \vec{A} \tag{3}$$

The magnetic vector potential due to an arbitrary shaped surface current density is shown in (4).

$$\vec{A} = \frac{\mu_0}{4\pi} \int_V G(r, r') \vec{J}(r') dV' \quad (4)$$

If regions of different permeability are present, their effects can be accounted for by surface current whose density is given in (5), where M represents the magnetization of the media [10].

$$\vec{K}_f = \vec{M} \times \hat{n} \quad (5)$$

The contribution to the magnetic vector potential due to an equivalent magnetization current is given by an integral over the surface

$$\vec{A}^K = \frac{\mu_0}{4\pi} \int_S G(r, r') \vec{K}_f(r') dS' \quad (6)$$

To determine K there remains only to enforce the boundary conditions regarding the jump in H and B across the interface.

$$\hat{n} \times (\vec{H}_2 - \vec{H}_1) = 0 \quad (7)$$

or

$$\hat{n} \times \left(\frac{\vec{B}_2}{\mu_2} - \frac{\vec{B}_1}{\mu_1} \right) = 0 \quad (8)$$

Before applying (8) one must take care to use the correct normal derivative expressions [11] [12], i.e., since $\hat{n} \times (\vec{H}_2 - \vec{H}_1) = \vec{K}_f$,

$$\frac{\partial A_2}{\partial n} = \mu_0 \int_{s'} \frac{\partial G(r', r)}{\partial n} K_f dS' - \mu_0 \frac{K_f}{2} \quad (9)$$

Combining (6) – (9) yields a single integral equation for the unknown fictitious surface current [13].

$$\mu_0 \int_{s'} \frac{\partial G(r, r')}{\partial n} \vec{K}_f dS' + \frac{1 + \mu}{1 - \mu} \frac{\mu_0 \vec{K}_f(r)}{2} = B_t(s) \quad (10)$$

where $\mu = \frac{\mu_1}{\mu_2}$ and \vec{B}_i is the tangential B field due to all other external magnetic sources. If the media is nonlinear internal volume currents must be added to account for $\nabla_x \vec{M}$ and iteration of (10) is necessary until the local permeability assumed is correct [14].

Verification of Numerical Simulation

By way of determining the accuracy of the simulation a ferrite torroid was placed in a saline solution as shown in Figure 2.

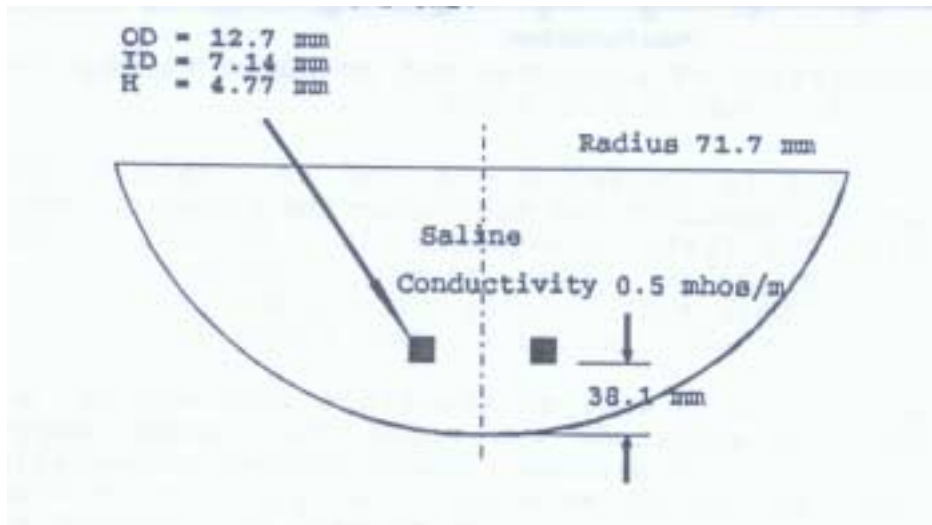


Figure 2: Experimental placement of small torroid in a saline tank. The core is excited at 15 kHz and the field measured along the primary axis.

The core is wound with 11 turns of #22 enamel wire and excited with a sinusoidal 10 volt signal at 5 kHz. A dipole probe with tips spaced 7 mm is employed to measure the voltage along the axis. The signal is fed into an isolated low noise Grass amplifier to record the voltage. Since the core is excited a current levels below saturation, the flux in the core can be either calculated as the MMF divided by the voltage, or measured as the voltage on a one turn test coil divided by the frequency ω .

The E field is predicted as outlined above the integrated over the 7 mm length spanned by the probe tips. The accuracy of this approach is defended by the results shown in Figure 3.

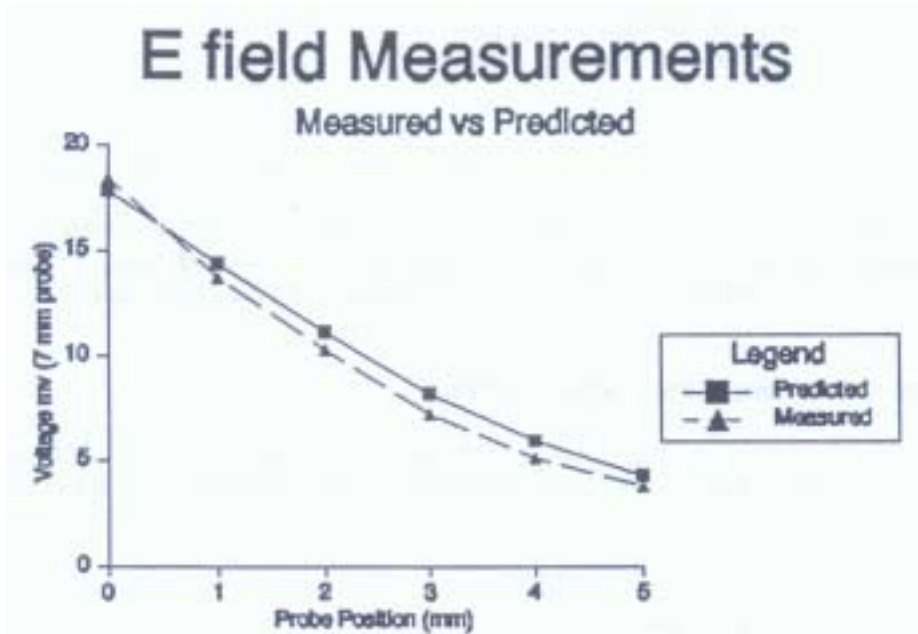


Figure 3: Correlation of predicted and measured voltage when the ferrite torroid is excited at 5 kHz.

As the torroid is lowered in the bowl to within 0.3125 mm of the bottom, the influence of the nonconducting boundary reduces the induced E field. The field is measured along the axis moving away from the bottom of the container. Figure 4 shows the accuracy of the prediction in this test. Notice that although the current is greatly impacted in this position, the field is only slightly reduced.

Both the E field as well as the field gradient are shown in Figure 5. The low magnitude motivated the design suggestions presented in the previous section, namely higher permeability core material, higher saturation material, and a partial occlusion of the central region of the torroid to channel the current and thus enhance the field gradient.

As witnessed by the field plot of Figure 6, the E field gradient is greatly augmented with the occlusion present. The larger test core setup is shown in Figure 7.

The agreement between predicted and measured fields continues to remain strong as shown in Figure 8.

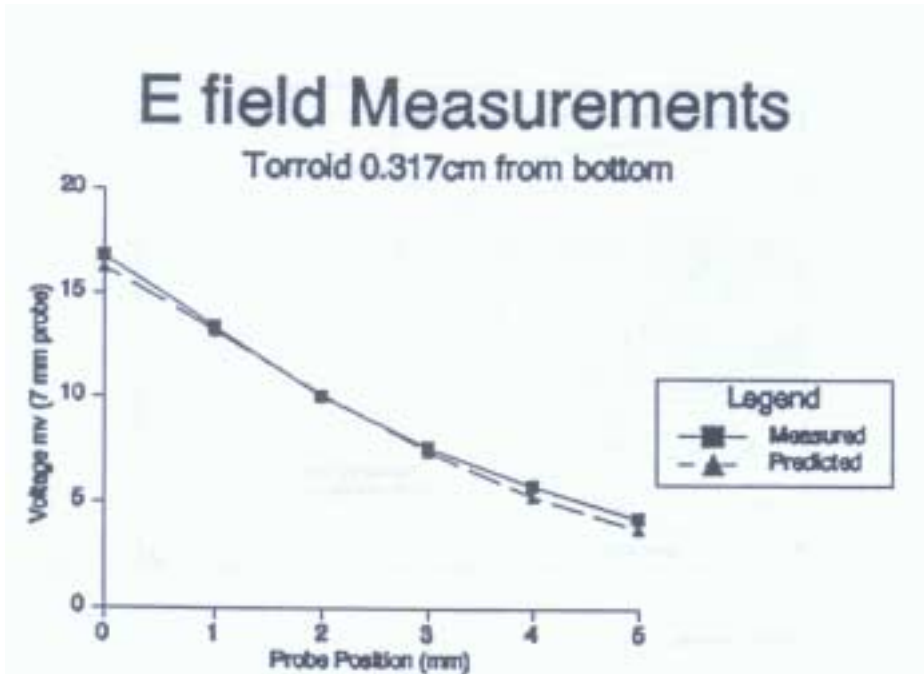


Figure 4: Induced field as the torroid core is lowered to within 0.3125 cm of the bottom of the test bath.

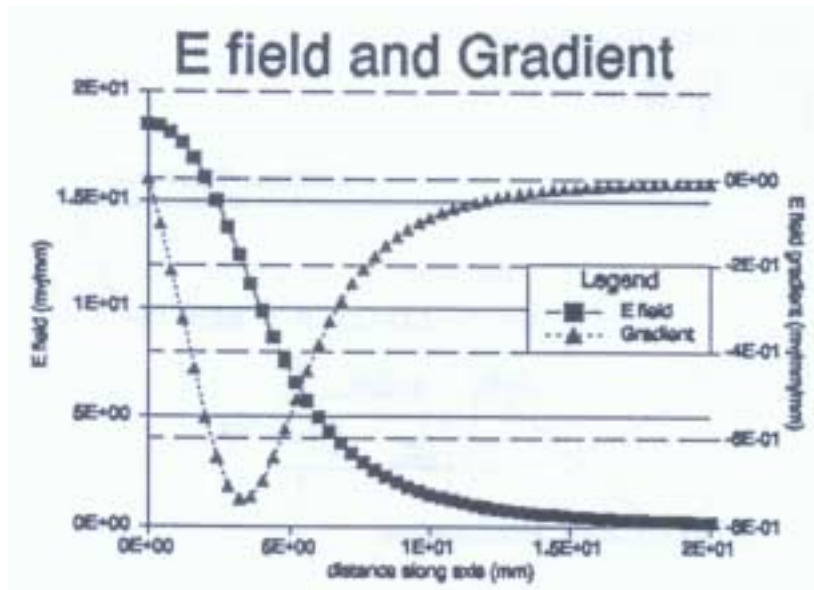


Figure 5: E field and gradient predicted with a small unoccluded ferrite core.

The new E field and gradient prediction for this core is shown in Figure 9. Smaller cores can be used if stronger μ materials such as vanadium permendur are employed. With all these materials except ferrite, the core must be laminated to avoid eddy current losses.

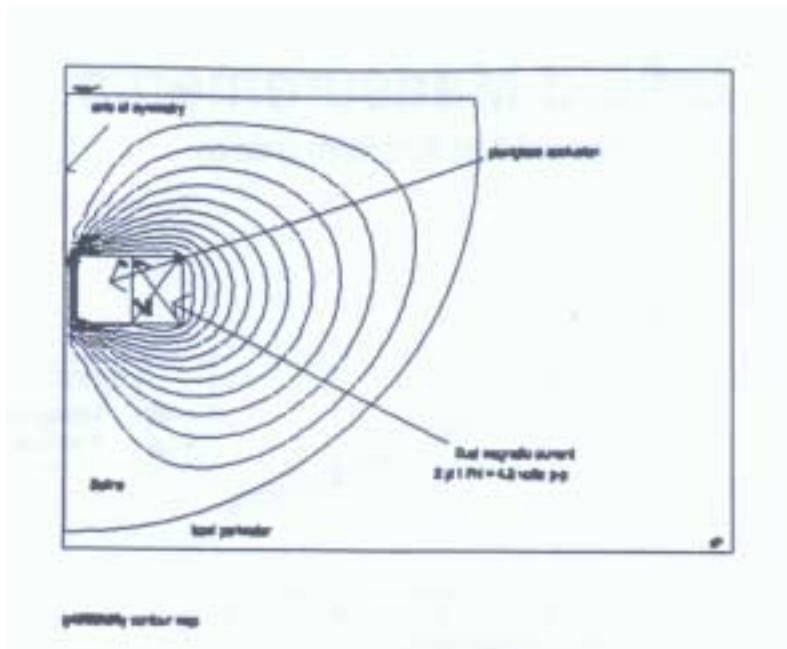


Figure 6: Field plot showing the concentration of current in the center of an occluded core.

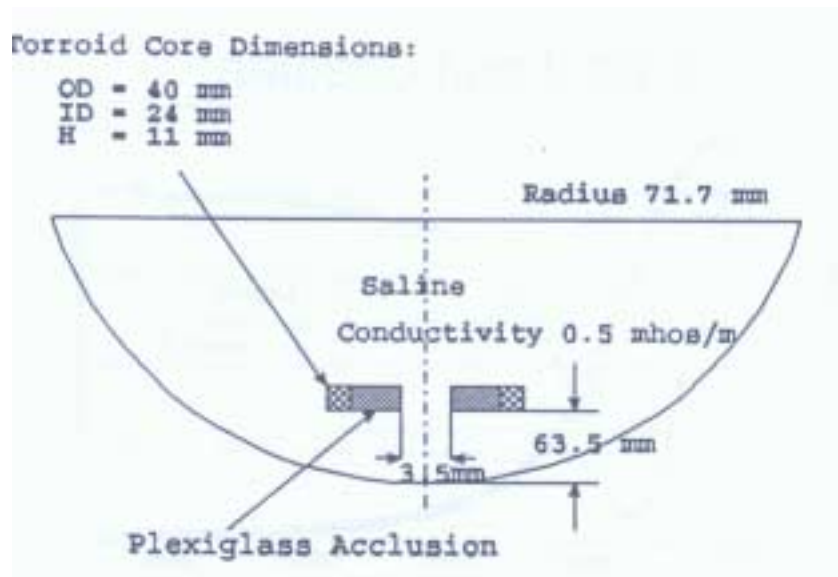


Figure 7: Occluded orthinol test core setup. The central region of the core is sealed with a plexiglass filler, leaving a 3.5 mm central orifice.

Nerve Enervation Tests

E field Measurements

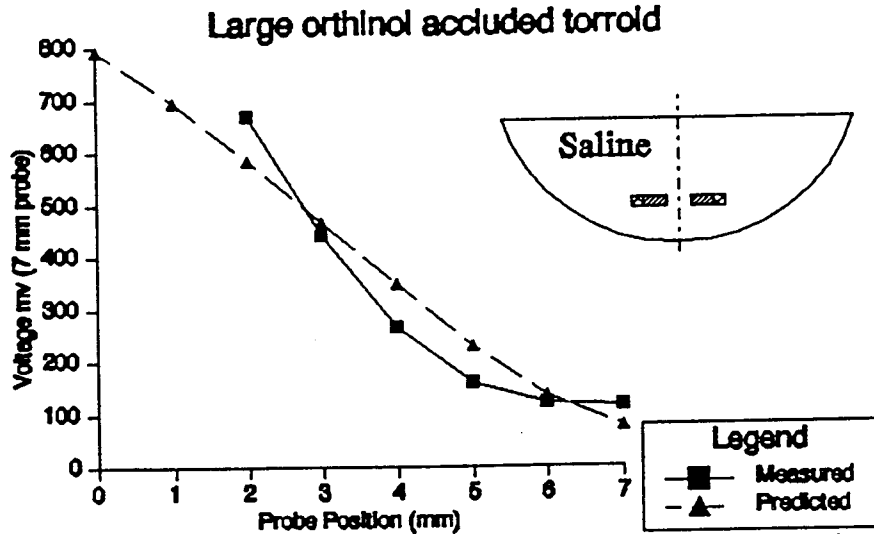


Figure 8: Measured and predicted fields in a core with a central occlusion.

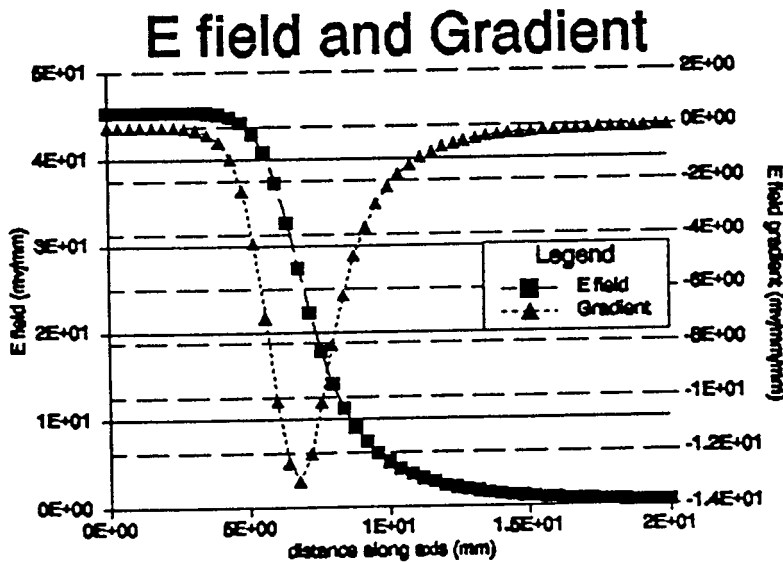


Figure 9: E field and gradient for the orthinol core with occlusion.

The cores were tested on African bullfrogs. A sciatic nerve preparation was made cutting the proximal end of the nerve closest to the hip, leaving the distal end in tact. The working length of the nerve was about 2.5 cm. Since torroid cores were used, the loosed end was threaded through the central orifice. Enervation was witnessed visually by muscle movement. Two cores were used in these experiments – the large orthinol core, the dimensions of which are specified in Figure 7 occluded with a 0.3175 mm orifice, and a smaller vanadium permendur core having dimensions

ID=1.27 cm, OD=1.905 cm, H=0.635 cm, occluded with a 1.9 mm orifice. Each experiment was run over a number of frequencies. In each case the current, voltage on the coil, core flux, power loss in the coil, E field at the hole, and the E field gradient at the hole were recorded. The large orthinol core was wound with 9 turns while the small orthinol core had 11 turns. The results for the large orthinol core are shown in Table II, followed by the small vanadium core in Table III. The results reflect excitation levels at threshold excitation. For each new frequency, the amplitude was raised slowly from subthreshold excitation and then dropped as soon as a stimulus was observed. The results reported represent peak-peak quantities, except V and I which are RMS.

Table II Larger Orthinol core results

f kHz	V (mv)	I amps	Flux μ webers	Power Loss mW	E at Hole mV	$\frac{\partial E}{\partial x}$ at hole mV/mm ²
10	9.6	0.332	50.5	8.49	94.3	15.3
7.5	6.7	0.332	49	8.49	64.3	14.4
5	4.6	0.313	52.2	7.54	43.1	12.6
4	3.3	0.28	46.7	6.04	22.4	6.8
3	1.6	0.261	34.7	5.25	16.7	4.3
2	1	0.2	31.4	3.08	10	2.5
1	0.6	0.175	37.4	2.36	6	1.6
0.5	0.36	0.16	49.3	2	4	1.1
0.25	0.248	0.148	73	1.69	3	0.9
0.1	0.158	0.14	135	1.51	2.1	0.3

Table III Smaller Vanadium Permendur Core Results

f kHz	V (mv)	I amps	Flux μ webers	Power Loss mW	E at Hole mV	$\frac{\partial E}{\partial x}$ at hole mV/mm ²
10	6.82	0.709	36	33.18	134.6	20.5
7.5	4.93	0.46	34.6	14.0	97	16.8
5	3.2	0.211	32.3	2.94	60	15
3	1.2	0.021	17	0.03	20.3	7.5
2	0.686	0.017	14.7	0.02	11.3	4.2
1	0.564	0.015	25.3	0.015	9.7	2.9
0.5	0.292	0.012	27.8	0.01	5.3	1.3
0.250	0.153	0.011	46.1	0.008	4.4	0.9

Recall that the cores are being driven sinusoidally. At the lower frequencies, the efficiency of charge transfer across the membrane is clearly witnessed by the lower E field gradient required to excite the nerve. Second, observe that the smallest core excitation flux in both cases is realized at 2 kHz. Third, observe the power requirements registered. In practice the sinusoidal signal would be active for a cycle and then quiet for 10-100 cycles to avoid muscle fatigue; such an excitation paradigm would reduce the power load by the duty cycle. This low power load would be necessary for implantable devices. Clearly the smaller occlusion also has a great bearing on the efficiency.

The low voltages suggest stimulation from small battery powered units. Several LC oscillator circuits offer promise in filling this role.

Conclusions

The results suggest a promising alternative to conventional FES. Peripheral nerves are shown to effectively stimulate with low threshold excitation levels. Several questions remain to be addressed in future research, among those being the following:

1. A folded toroid is the only practical unit for long term use in vivo. How well does this alternate geometry perform?
2. Although the unit is not in direct contact with the nerve, it must still be in close proximity. How will the nerve handle the mechanical load of the core in close proximity to the nerve bundle?
3. Two units with fluxes anti-parallel can be used to generate a hyperpolarizing potential on the outboard regions of the nerve, with a polarizing potential in the central region. Preliminary laboratory results have been performed and agree well with numerical calculations. How can such multiple units be employed to preferentially stimulate smaller nerve fibers to the exclusion of the larger ones in a bundle?

Acknowledgements

This work was supported by the Veterans Administration under the auspices of the Atlanta Rehab R&D unit in Decatur, GA. The magnetic field calculations were performed by a boundary element solver "Magneto" from Integrated Engineering Software in Winnipeg, Canada.

References

1. V.E. Amassian, R.Q. Cracco, and P.J. Maccabee, "Basic Mechanisms of Magnetic coil excitation of nervous system in humans and monkeys and their applications", Proceedings of a special Symposium on Maturing Technologies and Emerging Horizons, IEEE EMBS, 10th Annual Conference, pp 10-17, 1988.
2. A.T. Baker, I.L. Freeston, R. Jalinous, and J.A. Jaratt, "Magnetic Stimulation of the Human Brain and Peripheral Nervous System: An Introduction and the results of an Initial Clinical Evaluation", Neurosurgery, 20, pp 100-109, 1987.
3. B.J. Roth, L.J. Cohen, M. Hallett, W. Friauf, and P.J. Basser, "A Theroetical Calculation of the electric field induced by magnetic stimulation of a peripheral nerve", Muscle & Nerve, 13, pp 734-741, August, 1990.

4. K. Davey, C.H. Cheng, and C.M. Epstein, "Prediction of magnetically induced electric fields in biological tissue", *IEEE Trans. Biomedical Engr.*, vol 38, no 5, pp 418-422, May 1991.
5. S. McCarthy and D. Harradem, "Induced Current Constraints and Capacitive Effects in Induced Nerve Stimulation", *IEEE Trans Biomedical Engr*, vol 37, no 6, pp 598-605, June 1990.
6. B.J. Roth and P.J. Basser, "A model of the stimulation of a nerve fiber by electromagnetic induction", *IEEE Trans Biomedical Engr*, vol 37, no 6, pp 588-957, June 1990.
7. E.N. Warman, W.M. Grill, D. Durand, and J.T. Mortimer, "A new formulation of the activation function for estimation of neural excitation thresholds", *Proc. Of the 13th Annual IEEE EMBS conference*, no 2, pp 916-917, 1991.
8. R. Plonsey and R. Barr, *Bioelectricity – A Quantitative Approach*, Plenum Press, New York, pp 138-141, 1991.
9. Roger F. Harrington, "Boundary Integral Formulations for Homogeneous Material Bodies", *J. Electromagnetic Waves and Applications*, vol 3, #1, 1989, pp 1-15.
10. J.A. Stratton, *Electromagnetic Theory*, New York:, McGraw Hill Book Co., 1941.
11. Bruce W. Klimpke, *A Two Dimensional, Multi Media Boundary Element Method*, PhD Dissertation, University of Manitoba, 1983.
12. Y.B. Yildir, *A Boundary Element Method for the Solution of Laplace's Equation in Three Dimensional Space*, Ph.D. Dissertation, University of Manitoba, 1985.
13. Meng H. Lean, "Application of Boundary Element Methods to Electromagnetics", *IEEE Trans. Magnetics*, vol MAG-21, No 5, 1985, pp 1823-1828.
14. Meng H. Lean and Dan S. Bloomberg, "Nonlinear Boundary element Method for Two Dimensional Magnetostatics", *J. Appl. Phys.*, 55 (6), 1984, pp 2195-2197.